TISSUE ENGINEERING: Part A
Volume 27, Numbers 23 and 24, 2021

DOI: 10.1089/ten.tea.2021.0049

termis
Tissue Engineering
& Regenerative Medicine
International Society

ORIGINAL ARTICLE

Combining a Vascular Bundle and 3D Printed Scaffold with BMP-2 Improves Bone Repair and Angiogenesis

Toshiyuki Kawai, MD, PhD,[1,2] Chi-Chun Pan, PhD,[1,3] Yaichiro Okuzu, MD, PhD,[2]
Takayoshi Shimizu, MD, PhD,[2] Alexander M. Stahl, PhD,[1,4] Shuich Matsuda, MD, PhD,[2]
William J. Maloney, MD,[1] and Yunzhi P. Yang, PhD[1,5,6,*]

Vascularization is currently considered the biggest challenge in bone tissue engineering due to necrosis in the center of large scaffolds. We established a new expendable vascular bundle model to vascularize a three-dimensional printed channeled scaffold with and without bone morphogenetic protein-2 (BMP-2) for improved healing of large segmental bone defects. Bone formation and angiogenesis in an 8 mm critical-sized bone defect in the rat femur were significantly promoted by inserting a bundle consisting of the superficial epigastric artery and vein into the central channel of a large porous polycaprolactone scaffold. Vessels were observed sprouting from the vascular bundle inserted in the central tunnel. Although the regenerated bone volume in the group receiving the scaffold and vascular bundle was similar to that of the healthy femur, the rate of union of the group was not satisfactory (25% at 8 weeks). BMP-2 delivery was found to promote not only bone formation but also angiogenesis in the critical-sized bone defects. Both insertion of the vascular bundle alone and BMP-2 loading alone induced comparable levels of angiogenesis and when used in combination, significantly greater vascular volume was observed. These findings suggest a promising new modality of treatment in large bone defects.
Level of Evidence: Therapeutic level I.

Keywords: bone tissue engineering, skeletal defect, vascular bundle, recombinant human bone morphogenetic protein 2, animal model, 3D printing

Impact Statement

Vascularization is currently the main challenge in bone tissue engineering. The combination of a vascular bundle and an osteoinductive three-dimensional printed graft significantly improved and accelerated bone regeneration and angiogenesis in critical-sized large bone defects, suggesting a promising new modality of treatment in large bone defects.

Introduction

The repair of large skeletal defects resulting from severe trauma, fracture nonunion, or tumor resection remains a significant clinical challenge. A common practice to treat skeletal defects larger than 5 cm is vascularized autologous bone graft,[1–4] because it provides osteogenic cells, osteoinductive factors, and osteoconductive matrix that are supplied by a vascular network. However, the limited supply of vascularized autograft, longer surgical time, complexity of the procedure, and donor site morbidity are obstacles toward its practicality. Non-vascularized autologous bone graft is also an option to reconstruct bone defects, but it is limited to smaller defects due to lack of blood supply.[5–7] Allograft bone is another alternative that is more abundant in supply than autologous bone grafts, but it is more prone to nonunion (11–44%).[8–13]

Bone tissue engineering (TE) has emerged as a promising alternative source of bone grafts that are capable of addressing the limitations associated with current therapeutic techniques. Currently, vascularization is considered the biggest challenge in bone TE,[14] because cells cannot survive

[1]Department of Orthopaedic Surgery, Stanford University, Stanford, California, USA.
[2]Department of Orthopaedic Surgery, Kyoto University, Kyoto, Japan.
Departments of [3]Mechanical Engineering, [4]Chemistry, [5]Materials Science and Engineering, and [6]Bioengineering, Stanford University, Stanford, California, USA.

when located more than 200 μm away from the nearest capillary,[15–17] which is below the resolution of current large construct fabrication technologies. If an avascular engineered construct is implanted *in vivo*, blood vessels from the surrounding host tissue can only progress into the scaffold at a rate of several tenths of a micrometer per day,[18–20] which is inadequate to deliver nutrients and oxygen into the center of large scaffolds.

Some researchers have introduced vascular bundles into scaffolds made of calcium phosphate,[21–26] synthetic organic polymers,[27] or composites of the two[28,29] as a means to enhance vascularization and bone formation within the scaffolds.[30,31] Grafts with incorporated vascular bundles have shown greater vascularization and osteogenesis in bone models in rats,[32] rabbits,[25,27] and sheep.[22] However, the vascular bundles used in the majority of studies (the femoral artery[25] and radial artery[27]) cannot be sacrificed in clinical practice. In this study, we proposed a new model using an expendable vascular bundle comprising the superficial epigastric artery (SEA) and vein (SEV) and examined their efficacy in bone healing and vascularization in a critical-sized bone defect. The epigastric artery is one of the supplier arteries for superficial tissue of the lower abdomen. As it has collateral arteries such as the superior and inferior epigastric arteries,[33] this artery is regarded as one of the expendable arteries that can be sacrificed or embolized.[34]

We previously systematically developed and characterized three-dimensional (3D) printed polycaprolactone/β-tricalcium phosphate (PCL/β-TCP) scaffolds[35–37] and successfully applied these scaffolds in large segmental bone defect repair in rats.[38] We have also characterized the dosage effect of recombinant human bone morphogenetic protein-2 (BMP-2) on bone regeneration in a rat large segmental bone defect.[39] In the present study, we established a new model by creating an expendable vascular bundle comprising the SEA and SEV, and we examined the combined effects of a vascular bundle and BMP-2 loading in 3D printed channeled PCL scaffolds on bone healing and vascular formation in a critical-sized segmental defect in the rat femur. We hypothesized that the combination of both a vascular bundle and rhBMP-2 delivery within the scaffold would promote vascularization and osteogenesis, supporting survival and healing of the TE bone graft. Further, this model can provide a new strategy for treating femoral bone defects in clinical practice, because the SEA and SEV are expendable vessels.

Materials and Methods

Scaffold preparation

Medical-grade PCL pellets (Sigma-Aldrich Chemical Company, St. Louis, MO) with a density of 1.145 g/cm^3 (Mn.80,000) were used as received. A central channel-containing porous biodegradable PCL cylindrical scaffold with 4 mm diameter and 8 mm length was designed to be tested in a rat segmental bone defect model. The longitudinal central tunnel with a diameter of 2 mm was designated to accommodate the blood bundle insertion during implantation. A custom G-code generator written in Python was used to design the cylindrical scaffolds (2 mm inner diameter, 4 mm outer diameter, and 8 mm in length) since open-source G-code generators such as Slic3r were unable to create a printable design due to excessive porosity and restrictive dimensions. The generator took inputs for layer height, strut size, temperature, and print speed, which were set to 300 μm for both layer height and strut size, 140°C, and 1 mm/s, respectively. The scaffold design consisted of an alternating layer-by-layer pattern that resulted in a central tunnel, as shown in Figure 1, which was optimized for printability, structural integrity, and high porosity. The generated G-code was then exported to Repetier-host (Hot-World GmbH & Co. KG), which controls our custom 3D printing platform, Hybprinter, to fabricate the final scaffold. Before fabrication, the print head was preheated to 140°C until the filament could be extruded smoothly; the G-code for the scaffold was loaded and run after the preheating process. The print speed was set at 1 mm/s to ensure successful attachment of molten filament to previous layers. Meanwhile, the cooling fan was on during printing. After the scaffold was printed, it was left on the printing stage for a minute to ensure its structure was stable before we removed it from the stage. Finally, redundant struts on scaffold were trimmed off before the surface treatment. After 3D printing, all scaffolds were surface-treated with 5M NaOH for 12 h at room temperature to enhance their hydrophilicity and microroughness on the strut surface based on the methods in previous reports.[40,41] Images of the scaffolds were

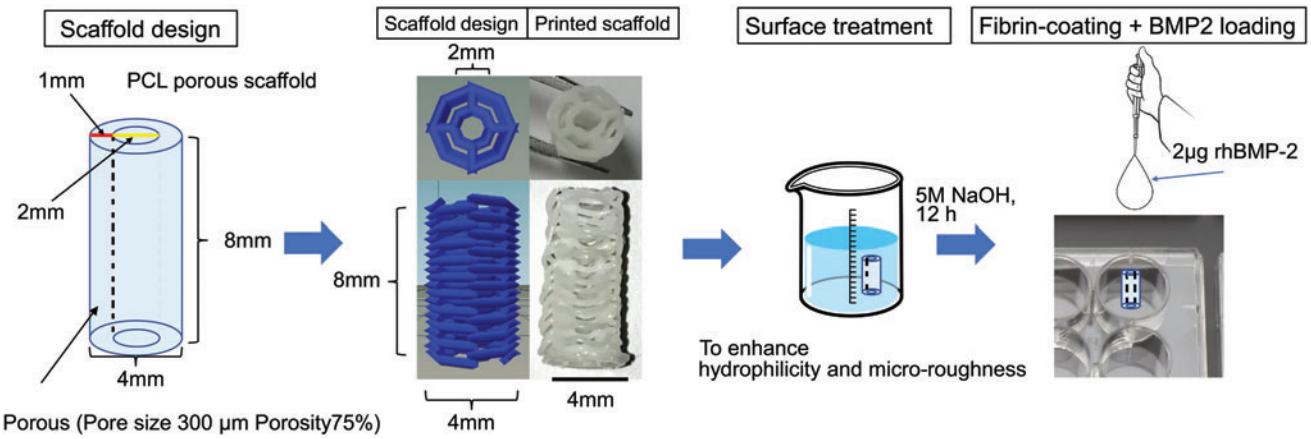

FIG. 1. The design of the 3D printed PCL scaffold. 3D, three-dimensional; PCL, polycaprolactone. Color images are available online.

taken to evaluate pore size, porosity, height, channel diameter, and strut size, which were determined by using the measuring tools in GIMP 2.0 ($n=3$). The porosity and strut size were estimated by imaging analysis. For rhBMP-2 loading, scaffolds were first soaked in a 1 mg/mL solution of fibrinogen for 24 h at 37°C and washed thrice with sterile PBS. Next, they were soaked in a 4 U/mL solution of thrombin for 2 h at 37°C and washed thrice with sterile PBS. Finally, the scaffolds were loaded with 10 μL of a 0.2 mg/mL rhBMP-2 solution, for a total of 2 μg rhBMP-2 per scaffold.[39] The scaffolds were then stored overnight in tissue culture plates at 4°C and were used for animal experiments the next day.

Animal groups

Fifty-six male Sprague-Dawley rats (Charles River Laboratories, Inc., Stone Ridge, NY), weighing from 320 to 450 g, were used to analyze bone defect healing and vascular prevalence in four experimental groups: Group 1 was the scaffold alone, labeled as Sca ($n=12$); Group 2 was the scaffold with an inserted vascular bundle, labeled as Sca+VB ($n=12$); Group 3 was the BMP-2 loaded scaffold, labeled as Sca+BMP-2 ($n=12$); and Group 4 was the BMP-2 loaded scaffold with an inserted vascular bundle, labeled as Sca+VB+BMP-2 ($n=12$). As a control, eight rats that underwent no surgery were used to analyze bone and vascular volumes in intact femurs. All experiments with animals were approved and performed following Stanford University Animal Care and Use Committee guidelines.

Surgical procedure

Anesthesia was induced and maintained with isoflurane (5% for induction and 2% for maintenance, with 2 L/min oxygen flow). Analgesia was administered by an injection of 0.5 mg/kg buprenorphine just before skin incision and twice daily for the first 2 days after surgery.

The surgical procedure was conducted as depicted in Figure 2. Using a lateral approach to the femur, a 2.5 cm incision was made through the skin (0.5 cm distal to the trochanter extending to ~0.5 cm above the femoral condyles). The fascia latae covering the thigh muscle was incised, and the vastus lateralis was retracted anteriorly from the intramuscular septum to expose the femur. The femur was plated internally via a rigid 22-mm-long polyether ether ketone fixation plate specifically developed for the rat femur. The plate was placed on the anterior cortex of the pre-determined defect site and fixed with four 1.1 mm diameter threaded k-wires that served as screws. After plating, an 8-mm wide segment was removed by transversely cutting the femur with a rotating diamond-coated blade.

A 2-cm incision was made on the ventral side of the thigh parallel to the common femoral artery. Using microsurgical techniques, the SEA and SEV, which are a branch of the femoral artery and vein, were identified as an expendable vascular bundle, elevated from the surrounding muscles, and ligated at 2.5 cm distal to the bifurcation from the femoral artery. In the Sca+VB Group and Sca+VB+BMP-2 Group, the bundle was inserted into the scaffold through the central tunnel. In the Sca Group and Sca+BMP-2, the vascular bundle was elevated and ligated and left at the original position. Then, the scaffold was placed into the bone defect. As the defect was created slightly smaller than the scaffold, so that the scaffold can press-fit into the bone defect, the scaffold was stable in the defect.

X-ray evaluation

The lateral radiographs of the femur were taken at 2, 4, 6, and 8 weeks after surgery by using the LAGO-X *in vivo* imaging system (Spectral Instrument Imaging, Tucson, AZ). The defect was regarded as healed when cortical continuity bridging the defect was confirmed.[42–44]

Micro computed tomography evaluation

Vascular formation in the hind limb was evaluated at 8 weeks by microangiography. A polymerizing contrast agent, Microfil (Flow Tech, Carver, MA), was injected under physiologic pressure via the abdominal aorta. Then, the thigh was harvested and examined by a micro computed tomography (CT) scan to quantify the volume of bone and blood vessels. The specimens were decalcified in 15% EDTA (pH 8.0) at 4°C. The decalcified specimens were

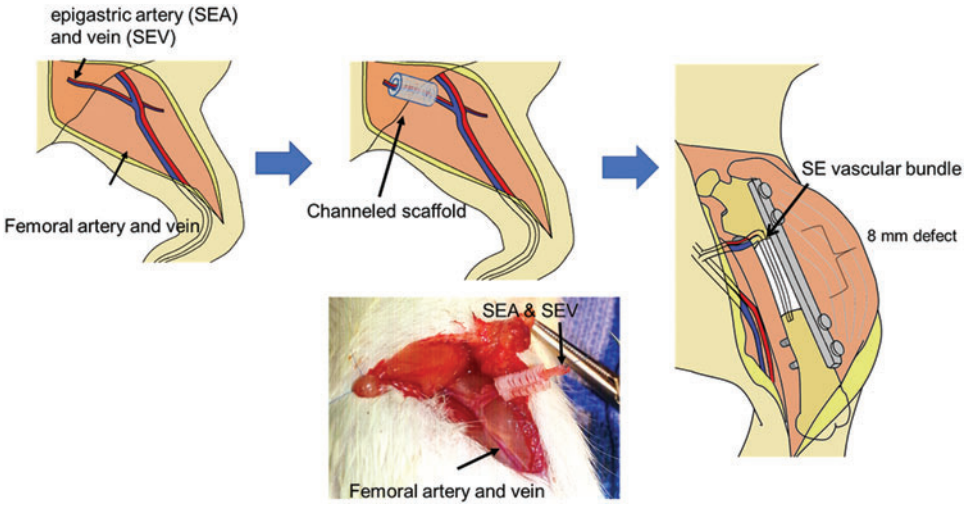

FIG. 2. Schematic images of the surgical procedure. Color images are available online.

subjected to micro CT scanning again for the quantification of vessels alone. A microfocus X-ray CT system (SMX100CT-SV3; Shimadzu Co., Kyoto, Japan) was used to acquire microstructural information about the proximal femurs at 8 weeks after the surgery. The entire set of radiographs was deconvoluted by computer software to reconstruct a 3D image of the microstructure with a voxel size of 12 μm and was evaluated by using 3D image-processing software VG studio MAX 2.0 (Volume Graphics, Heidelberg, Germany). A cylindrical region of interest (5.0 mm in diameter, 8 mm in length) was concentrically positioned over the defect site to measure bone formation and vessel volume in the entire defect area. Another cylindrical region of interest (2.0 mm in diameter, 8 mm in length) was positioned at the center of the porous body to measure vessel volume in the central tunnel of the porous body. The location of the original defect site was easily confirmed based on the location of k-wires. The volume of new bone and vessels was determined by the software. Thresholds were applied to differentiate between new bone and residual scaffold material in the region of interest, as previously reported.[45]

Histology

The specimens were fixed in 10% phosphate-buffered formalin (pH 7.25) for 3 days, and they were dehydrated in serial concentrations of ethanol (70%, 80%, 90%, 99%, 100%, and 100% v/v; 1 day in each). The specimens were then embedded in polyester resin. Thick sections (250 mm) were cut with a band saw (BS-3000CP; EXACT cutting system, Norderstedt, Germany) perpendicular to the axis of the implant, and they were ground to a thickness of 40–50 mm by using a grinding-sliding machine (Microgrinding MG-4000, EXACT). Each section was then stained with Stevenel's blue and Van Gieson's picrofuchsin. Microscopic analysis was performed on histological slides by using transmitted light microscopy (Nikon Model Eclipse 80i) combined with a digital camera (Nikon Model DS-5M-L1).

Statistical analysis

Differences in means were calculated by the Kruskal-Wallis test followed by the *post hoc* Steel-Dwass test. Probability values <0.05 were considered significant.

Results

Based on image processing, the completed 3D printed scaffolds measured 8.10 ± 0.17 mm in height and 4.17 ± 0.19 mm in outer diameter. The diameter of the central channel was 1.44 ± 0.04 mm, the strut size was 299 ± 17 μm, the pore size of the scaffold was 203 ± 39 μm, and the porosity of the scaffold was $\sim 64.3\% \pm 3.0\%$. Variation in the pore size within the scaffolds was caused by the resolution of the motor (50 μm) and the cooling of PCL struts. As the overall scaffold dimensions were small, any fluctuation could induce a relatively large difference in pore size (203 ± 39 μm).

Bone union in the 8 mm defect created in rat femur was confirmed in 0 out of 12 (0%) rats in the Sca Group (the scaffold alone), 2 out of 12 (16.7%) rats in the Sca+VB Group (the scaffold with an inserted vascular bundle), 11 out of 12 (91.7%) rats in the Sca+BMP-2 Group (the BMP-2 loaded scaffold), and 11 out of 12 (91.7%) rats in the Sca+VB+BMP-2 Group (the BMP-2 loaded scaffold with an inserted vascular bundle) at 4 weeks. Representative x-rays are shown in Figure 3. At 8 weeks, union rate was the same as at 4 weeks in the Sca Group, the Sca+BMP-2 Group, and the Sca+VB+BMP-2 Group, but it increased to 3 out of 12 (25%) in the Sca+VB Group.

The amount of new bone formation in the defect area after 8 weeks was $25.3 \pm 12.8\,mm^3$ for the Sca Group, $46.9 \pm 22.8\,mm^3$ for the Sca+VB Group, $80.3 \pm 22.7\,mm^3$ for the Sca+BMP-2, and $87.7 \pm 15.6\,mm^3$ for the Sca+VB+BMP-2 Group ($n = 12$). The bone volume measured in the same area of the intact femoral control was $44.1 \pm 5.0\,mm^3$ ($n = 8$). Statistically significant differences were found between any two experimental groups among the four ($p = 0.016$ for the Sca Group vs. the Sca+VB Group, $p < 0.001$ for the Sca Group vs. the Sca+BMP-2 Group, the Sca Group vs. the Sca+VB+BMP-2 Group, the Sca+VB Group vs. the Sca+BMP-2 Group, and the Sca+VB Group vs. Sca+VB+BMP-2 Group) except between the Sca+BMP-2 Group and the Sca+VB+BMP-2 Group (Fig. 4a), which had no significant difference ($p = 0.67$ for the Sca+BMP-2 Group vs. the Sca+VB+BMP-2 Group). More specifically, the bone volumes in the Sca+BMP-2 Group and the Sca+VB+BMP-2 Group were significantly higher than that in the same area in the normal femoral bone ($p < 0.001$ for each comparison). There is no difference in bone volume between the Sca+VB Group and that in the same area in the normal femoral bone ($p = 0.95$). The regenerating bone volume in the Sca Group was lower than the normal bone, but the difference was not statistically significant ($p = 0.21$). However, the bone volume in the Sca Group was significantly lower than the other three groups.

The vascular volume found within the entire scaffold was $1.2 \pm 1.1\,mm^3$ in the Sca Group, $3.8 \pm 2.4\,mm^3$ in the Sca+VB Group, $5.3 \pm 2.0\,mm^3$ in the Sca+BMP-2 Group, and $8.2 \pm 2.5\,mm^3$ in the Sca+VB+BMP-2 Group ($n = 10$), whereas the vascular volume in the same area in the intact femoral bone control group was $1.6 \pm 1.2\,mm^3$ ($n = 8$). The Sca+VB Group and the Sca+BMP-2 Group contained significantly more vasculature in the scaffold than the Sca Group ($p = 0.014$ for the Sca Group vs. the Sca+VB Group, $p < 0.001$ for the Sca Group vs. the Sca+BMP-2 Group), but it was significantly less than the Sca+VB+BMP-2 Group ($p < 0.001$ for the Sca+VB Group vs. the Sca+VB+BMP-2 Group, $p = 0.0083$ for the Sca+BMP-2 Group vs. the Sca+VB+BMP-2 Group) (Fig. 4b). The vascular volume in the total scaffold in the Sca+BMP-2 Group and the Sca+VB+BMP-2 Group was significantly larger than that in the normal femoral bone ($p < 0.001$ for each comparison).

The volume of blood vessels in the central tunnel was $0.2 \pm 0.2\,mm^3$ in the Sca Group, $1.5 \pm 0.9\,mm^3$ in the Sca+VB Group, $1.6 \pm 0.7\,mm^3$ in the Sca+BMP-2 Group, and $2.5 \pm 1.0\,mm^3$ in the Sca+VB+BMP-2 Group ($n = 10$). The vessel volume in the same area in the intact femoral bone was $0.8 \pm 0.7\,mm^3$ ($n = 8$). The Sca Group had a significantly smaller volume of vasculature in the central tunnel compared with the other three experimental groups ($p = 0.0040$ for the Sca Group vs. the Sca+VB Group, $p < 0.001$ for the Sca Group vs. the Sca+BMP-2 Group, the Sca Group, and Sca+VB+BMP-2 Group). There was also a

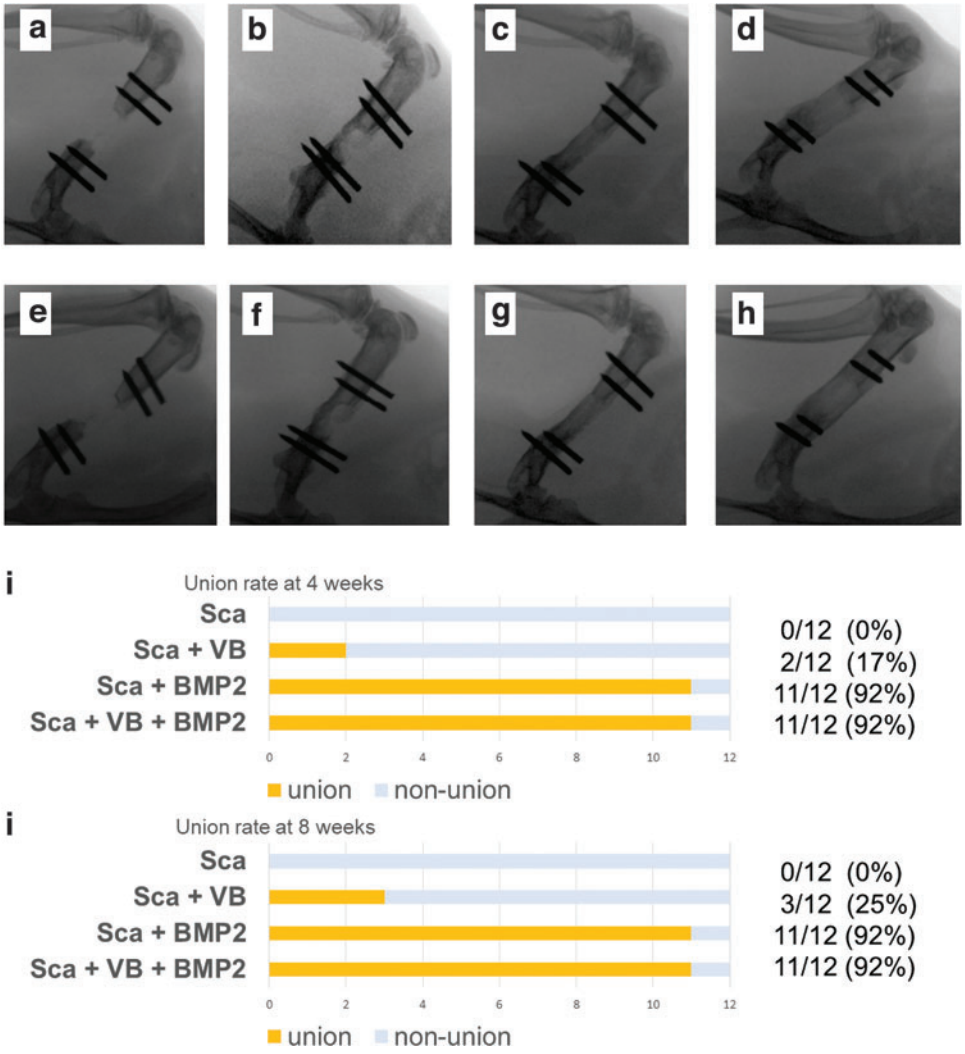

FIG. 3. X-rays taken at 4 weeks **(a–d)** and 8 weeks **(e–h)** after surgery. **(a)** Almost no bone formation was seen in Sca Group at 4 weeks. **(b)** Bone formation along the scaffold was observed in Sca+VB Group at 4 weeks. Complete bone bridging over the defect was seen in Sca+BMP-2 Group **(c)** and Sca+VB+BMP-2 Group **(d)** at 4 weeks. **(e)** Bone volume in the defect area was small in Sca Group at 8 weeks. **(f)** Considerably more bone formation was seen in Sca+VB Group at 8 weeks. The greatest bone formation was observed in Sca+BMP-2 Group **(g)** and Sca+VB+BMP-2 Group **(h)**. **(i)** Rate of bone union in the defect area at 4 weeks. **(j)** Rate of bone union in the defect area at 8 weeks. BMP-2, bone morphogenetic protein-2. Color images are available online.

significant difference in the amount of vasculature in the tunnel between the Sca+VB Group and the Sca+VB+BMP-2 Group ($p = 0.039$) (Fig. 4c). The vessel volume in the central tunnel in the Sca+VB+BMP-2 Group was significantly higher than that in the intact femoral bone ($p < 0.001$).

Micro CT images (Fig. 5) show that a large volume of bone was formed in the defect in the Sca+VB Group, the Sca+BMP-2 Group, and the Sca+VB+BMP-2 Group. In the Sca Group, only a small amount of bone was formed adjacent to the host bone, whereas in the Sca+VB Group, bone formed along the scaffold and a vessel-like structure could be seen in the central tunnel (Fig. 6c). In Figure 6, vessels can be seen sprouting from the vascular bundle inserted in the central tunnel in the Sca+VB Group and the Sca+VB+BMP-2 Group, and vessels can be seen invading from surrounding tissue into the scaffold in the Sca+BMP-2 Group. Histology images (Fig. 7) confirmed that a large volume of bone was formed in the Sca+VB Group, the Sca+BMP-2 Group, and the Sca+VB+BMP-2 Group, whereas only a small amount of bone was seen in the Sca Group. Vessel-like structures filled with Microfil were seen inside the central tunnel in the Sca+VB Group (Fig. 7c, d) and the Sca+VB+BMP-2 Group (Fig. 7g, h), whereas small vessel-like structures were seen throughout the entire scaffold in the Sca+BMP-2 Group (Fig. 7e, f). Vessel formation was limited to the area around the host bone in the Sca Group (Fig. 7a, b).

Discussion

In this study, we established a new expendable vascular bundle model to vascularize a 3D printed scaffold for improved healing of large segmental bone defects. We demonstrated that bone formation and angiogenesis were promoted by the insertion of an expendable branch of the femoral artery and vein, the epigastric artery and vein, into the center of a large scaffold. Although the regenerated bone volume in the group receiving the scaffold and vascular bundle (Sca+VB Group) was similar to that of intact normal femoral bones, the bone union rate of the group was not satisfactory (25% at 8 weeks). Regarding the use of a ligated vascular bundle, there have been several reports. Sever *et al.* reported that the insertion of a ligated artery into porous hydroxyapatite (HA) in rat thigh muscle increased vascularity and bone formation.[23] Wu *et al.* also reported that a scaffold prevascularized by insertion of a ligated vascular

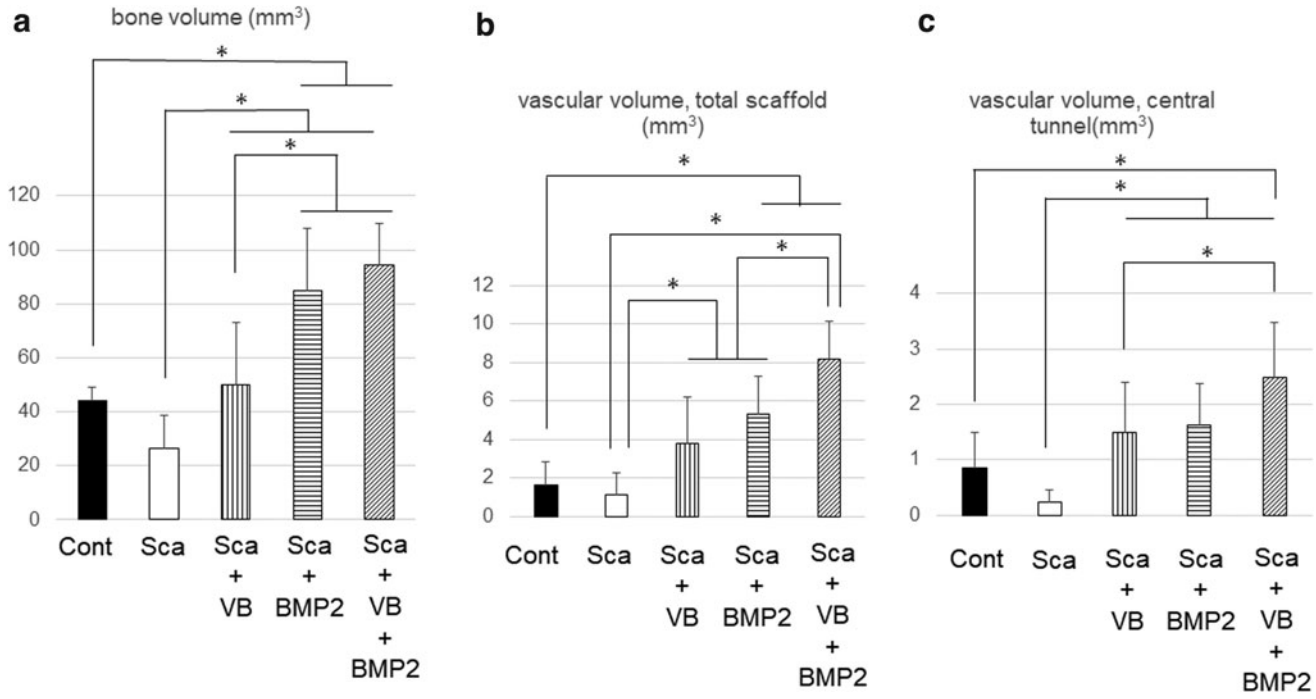

FIG. 4. **(a)** The amount of new bone formation in the defect area. **(b)** The vascular volume in the total scaffold. **(c)** The vascular volume in the central tunnel. $*p < 0.05$.

bundle had enhanced bone formation.[26] Akita *et al.* reported that ligated artery and vein inserted into porous HA in rat groin muscle enhanced bone formation.[24] Zhang also reported increased bone formation by using a ligated AV bundle into a polylactic acid-hydroxyapatite (PLA-HA) scaffold placed next to the tibia in rabbits.[28] Han *et al.* reported increased bone formation by a ligated vascular bundle insertion into PLA-HA scaffolds in the rabbit radius model.[27] The bone formation promoted in the Sca+VB Group in the present study was consistent with the results of those reports. However, the low union rate of our model may imply insufficiency in bone repair by the insertion of vascular bundle alone.

Some studies reported positive results on osteogenesis and angiogenesis after inserting a flow through the vascular bundle. Wang used a rabbit femoral bone defect model and demonstrated increased vascularity and enhanced bone formation after the insertion of a flow through the vascular bundle consisting of the deep femoral artery and vein into a beta-TCP porous body.[25] Li *et al.* compared the insertion of a scaffold+rhBMP-2 and a scaffold+rhBMP-2+AV bundle in rabbit thigh muscle and demonstrated increased angiogenesis and bone formation in the scaffold+rhBMP-2+AV bundle group.[29] In a pilot study of sheep metatarsal segmental bone defects, Vidal *et al.* found increased bone tissue regeneration in the animal receiving both 3D printed scaffold and inserted vascular pedicle.[22] From those findings, the flow though model seems a likely option to prevascularize a scaffold. However, the location where the flow through the bundle can be utilized is limited because it is

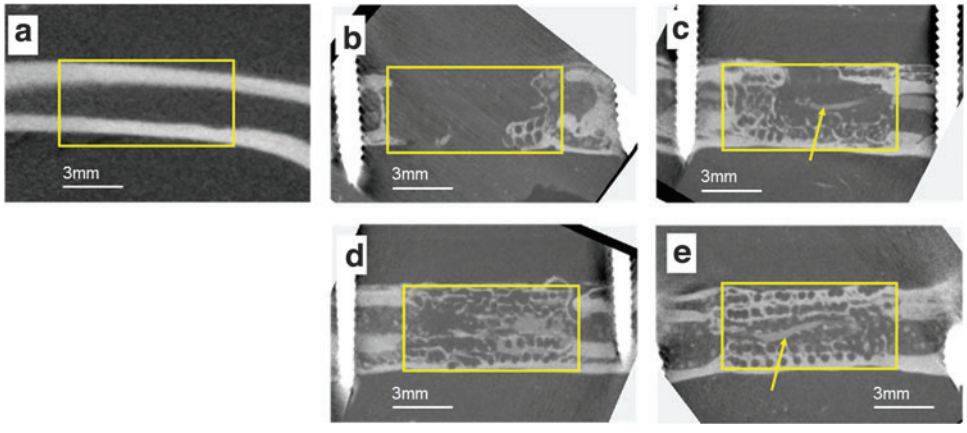

FIG. 5. Micro CT images after Microfil injection at 8 weeks after surgery. **(a)** Control femur without surgery. **(b)** Sca Group. **(c)** Sca+VB Group. **(d)** Sca+BMP-2 Group. **(e)** Sca+VB+BMP-2 Group. *Yellow boxes* for **(b–e)** indicate the location where the bone defect area was created, and the *yellow box* for **(a)** indicates the same location on the control bone. *Arrows* indicate a vessel-like structure filled with Microfil. CT, computed tomography. Color images are available online.

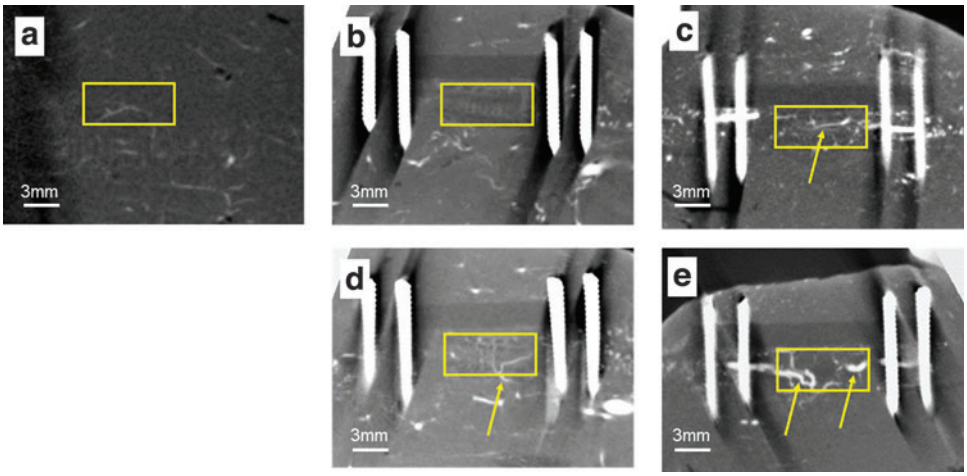

FIG. 6. Micro CT images after Microfil injection followed by decalcification, 8 weeks after surgery. **(a)** Control femur without surgery. **(b)** Sca Group. **(c)** Sca+VB Group. **(d)** Sca+BMP-2 Group. **(e)** Sca+VB+BMP-2 Group. *Yellow boxes* for **(b–e)** indicate the location where the bone defect area was created, and the *yellow box* for **(a)** indicates the same location on the control bone. *Arrows* indicate a vessel-like structure filled with Microfil. Color images are available online.

difficult to mobilize an artery without being ligated and elevated from surrounding tissue. Wu *et al.* compared the performance of a ligated vascular bundle and flow through a vascular bundle inserted into a porous β-TCP scaffold placed in the thigh muscle of beagle dogs. They reported that the ligated vascular bundle had more bone tissue whereas the flow through the vascular bundle had greater vascularity,[26] suggesting that prevascularization using a ligated vascular bundle could be a good treatment option for a large bone defect.

In the current study, we found that the loading of rhBMP-2 promotes not only bone formation but also angiogenesis in the critical-sized bone defects. Insertion of the ligated vascular bundle alone (Sca+VB Group) and rhBMP-2 loading alone (Sca+BMP-2 Group) generated almost the same volume of new vessel growth, and the combination of both the vascular bundle and rhBMP-2 had a significantly greater vascular volume. Several studies support the finding that BMP-2 can increase vessel formation. Pearson *et al.* demonstrated that the addition of BMP-2 promoted angiogenesis in a rat femoral defect, though BMP-2 did not directly stimulate angiogenesis *in vitro*.[46] Langenfeld and Langenfeld reported that BMP-2 promotes tube formation by human aortic endothelial cells and human umbilical vein endothelial cells.[47] Zuo reported that BMP-2 enhances HUVEC proliferation and migration.[48] The effects of BMP-2 demonstrated in this study were consistent with those

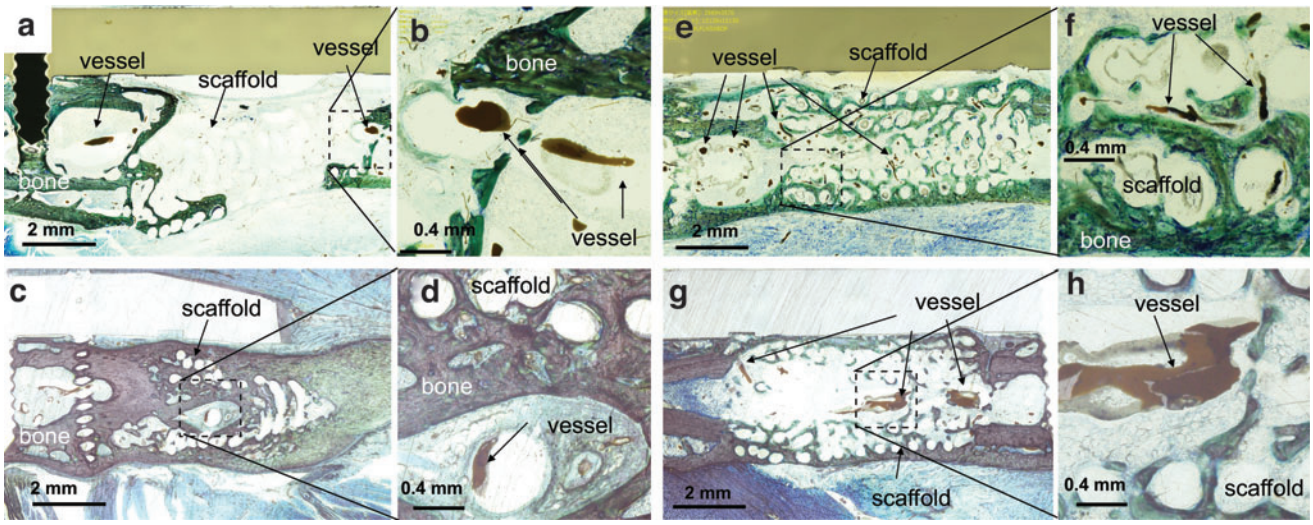

FIG. 7. Histology images stained with Stevenel's *blue* and Van Gieson's picrofuchsin. **(a, b)** Sca Group **(c, d)** Sca+VB Group. **(e, f)** Sca+BMP-2 Group, **(g, h)** Sca+VB+BMP-2 Group. **(b, d, f, h)** High magnification images of area indicated by *dashed boxes*. **(a, b)** Only a small amount of bone was observed along the scaffold in Sca Group. The formation of vessel-like structures was limited around the interface of the femoral bone and scaffold. There was almost no vessel formation inside the scaffold. **(c, d)** Bone formation was seen around the scaffold in Sca+VB Group. A vessel-like structure filled with Microfil was seen inside the central tunnel. **(e, f)** Bone formation bridging the defect was seen in Sca+BMP-2 Group. Small vessel-like structures filled with Microfil were observed throughout the scaffold. **(g, h)** Bone was growing along the scaffold in Sca+VB+BMP-2 Group. A vessel-like structure was seen in the central tunnel in the scaffold. Color images are available online.

previous studies. However, the release profile of BMP-2 eluting from the scaffold was not examined here, which is a limitation of the current study. Investigating the growth factor release profile would add valuable information in future studies.

The combination of the vascular bundle and BMP-2 had a synergistic effect on vascular formation. However, in this study, there was no significant difference in bone formation between the vascular bundle+BMP-2 group (Sca+VB+ BMP-2 Group) and the group receiving BMP-2 alone (Sca+BMP-2 Group). This could be because the BMP-2 dose employed in this study was high and masked the difference. Further study with lower doses of BMP-2 would be necessary to determine the relative contribution of the vascular bundle and BMP-2 on bone formation within the scaffolds. The lack of observed difference in bone formation might also be due to the relatively small size of rat femurs. A difference may be visible in large animal models, which will be our next avenue of inquiry. We also intend to determine whether a flow-through vascular bundle could further increase vascularity or bone formation.

We established a new expendable vascular bundle model to vascularize a BMP-2-eluting, 3D printed channeled scaffold for improved bone healing in large bone defects. The combination of a vascular bundle and BMP-2 improved both bone and vascular formation, suggesting an essential interplay between angiogenesis and osteogenesis. A preclinical large animal model could be further used to validate this clinically applicable approach by combining an expendable vascular bundle and 3D printed bone grafts for large bone defect repair.

Acknowledgment

The authors thank Angela Morben, DVM, ELS, from Edanz Group for editing a draft of this article.

Disclosure Statement

No competing financial interests exist.

Funding Information

This work was partially supported by NIAMS grants [grant numbers R01AR057837, U01AR069395, R01AR072613, R01AR074458], a DoD grant [grant number W81XWH-20-1-0343], Wallace H. Coulter Grants, the Uehara Memorial Foundation, JSPS KAKENHI [grant number JP 18K16622], and the Japan Hip Joint Foundation.

References

1. Pelissier, P., Boireau, P., Martin, D., and Baudet, J. Bone reconstruction of the lower extremity: complications and outcomes. Plast Reconstr Surg **111,** 2223, 2003.
2. Toh, S., Tsubo, K., Nishikawa, S., Narita, S., Kanno, H., and Harata, S. Ipsilateral pedicle vascularized fibula grafts for reconstruction of tibial defects and non-unions. J Reconstr Microsurg **17,** 487, 2001.
3. Muramatsu, K., Doi, K., Ihara, K., Shigetomi, M., and Kawai, S. Recalcitrant posttraumatic nonunion of the humerus: 23 patients reconstructed with vascularized bone graft. Acta Orthop Scand **74,** 95, 2003.
4. Mercado-Pagán, Á.E., Stahl, A.M., Shanjani, Y., and Yang, Y. Vascularization in bone tissue engineering constructs. Ann Biomed Eng **43,** 718, 2015.
5. Bumbasirevic, M., Stevanovic, M., Bumbasirevic, V., Lesic, A., and Atkinson, H.D.E. Free vascularised fibular grafts in orthopaedics. Int Orthop **38,** 1277, 2014.
6. Foster, R.D., Anthony, J.P., Sharma, A., and Pogrel, M.A. Vascularized bone flaps versus nonvascularized bone grafts for mandibular reconstruction: an outcome analysis of primary bony union and endosseous implant success. Head Neck **21,** 66, 1999.
7. Soucacos, P.N., Kokkalis, Z.T., Piagkou, M., and Johnson, E.O. Vascularized bone grafts for the management of skeletal defects in orthopaedic trauma and reconstructive surgery. Injury **44 Suppl 1,** S70, 2013.
8. Muscolo, D.L., Ayerza, M.A., Aponte-Tinao, L., Ranalletta, M., and Abalo, E. Intercalary femur and tibia segmental allografts provide an acceptable alternative in reconstructing tumor resections. Clin Orthop Relat Res **426,** 97, 2004.
9. Aponte-Tinao, L., Farfalli, G.L., Ritacco, L.E., Ayerza, M.A., and Muscolo, D.L. Intercalary femur allografts are an acceptable alternative after tumor resection. Clin Orthop Relat Res **470,** 728, 2012.
10. Bus, M.P.A., Dijkstra, P.D.S., van de Sande, M.A.J., *et al.* Intercalary allograft reconstructions following resection of primary bone tumors: a nationwide multicenter study. J Bone Joint Surg Am **96,** e26, 2014.
11. Enneking, W.F., and Campanacci, D.A. Retrieved human allografts: a clinicopathological study. J Bone Joint Surg Am **83,** 971, 2001.
12. Flierl, M.A., Smith, W.R., Mauffrey, C., *et al.* Outcomes and complication rates of different bone grafting modalities in long bone fracture nonunions: a retrospective cohort study in 182 patients. J Orthop Surg Res **8,** 33, 2013.
13. Donati, D., Capanna, R., Campanacci, D., *et al.* The use of massive bone allografts for intercalary reconstruction and arthrodeses after tumor resection. A multicentric European study. Chir Organi Mov **78,** 81, 1993.
14. Stahl, A., and Yang, Y.P. Regenerative approaches for the treatment of large bone defects. Tissue Eng Part B Rev 2020: [E-pub ahead of print]; DOI:10.1089/ten.TEB.2020.0281.
15. Jain, R.K., Au, P., Tam, J., Duda, D.G., and Fukumura, D. Engineering vascularized tissue. Nat Biotechnol **23,** 821, 2005.
16. Rouwkema, J., Rivron, N.C., and van Blitterswijk, C.A. Vascularization in tissue engineering. Trends Biotechnol **26,** 434, 2008.
17. Folkman, J., and Hochberg, M. Self-regulation of growth in three dimensions. J Exp Med **138,** 745, 1973.
18. Clark, E.R., and Clark, E.L. Microscopic observations on the growth of blood capillaries in the living mammal. Am J Anat **64,** 251, 1939.
19. Kang, K.-T., Allen, P., and Bischoff, J. Bioengineered human vascular networks transplanted into secondary mice reconnect with the host vasculature and re-establish perfusion. Blood **118,** 6718, 2011.
20. Osborn, S.L., So, M., Hambro, S., Nolta, J.A., and Kurzrock, E.A. Inosculation of blood vessels allows early perfusion and vitality of bladder grafts—implications for bioengineered bladder wall. Tissue Eng Part A **21,** 1906, 2015.
21. Beier, J.P., Horch, R.E., Hess, A., *et al.* Axial vascularization of a large volume calcium phosphate ceramic bone

substitute in the sheep AV loop model. J Tissue Eng Regen Med **4,** 216, 2010.
22. Vidal, L., Kampleitner, C., Krissian, S., *et al.* Regeneration of segmental defects in metatarsus of sheep with vascularized and customized 3D-printed calcium phosphate scaffolds. Sci Rep **10,** 7068, 2020.
23. Sever, C., Uygur, F., Kose, G.T., *et al.* Prefabrication of vascularized bone graft using an interconnected porous calcium hydroxyapatite ceramic in presence of vascular endothelial growth factor and bone marrow mesenchymal stem cells: experimental study in rats. Indian J Plast Surg Off Publ Assoc Plast Surg India **45,** 444, 2012.
24. Akita, S., Tamai, N., Myoui, A., *et al.* Capillary vessel network integration by inserting a vascular pedicle enhances bone formation in tissue-engineered bone using interconnected porous hydroxyapatite ceramics. Tissue Eng **10,** 789, 2004.
25. Wang, L., Fan, H., Zhang, Z.-Y., *et al.* Osteogenesis and angiogenesis of tissue-engineered bone constructed by prevascularized β-tricalcium phosphate scaffold and mesenchymal stem cells. Biomaterials **31,** 9452, 2010.
26. Wu, X., Wang, Q., Kang, N., *et al.* The effects of different vascular carrier patterns on the angiogenesis and osteogenesis of BMSC-TCP-based tissue-engineered bone in beagle dogs. J Tissue Eng Regen Med **11,** 542, 2017.
27. Han, D., and Li, J. Repair of bone defect by using vascular bundle implantation combined with Runx II gene-transfected adipose-derived stem cells and a biodegradable matrix. Cell Tissue Res **352,** 561, 2013.
28. Zhang, H., Mao, X., Zhao, D., *et al.* Three dimensional printed polylactic acid-hydroxyapatite composite scaffolds for prefabricating vascularized tissue engineered bone: an in vivo bioreactor model. Sci Rep **7,** 15255, 2017.
29. Li, B., Ruan, C., Ma, Y., *et al.* Fabrication of vascularized bone flaps with sustained release of recombinant human bone morphogenetic protein-2 and arteriovenous bundle. Tissue Eng Part A **24,** 1413, 2018.
30. Sparks, D.S., Savi, F.M., Saifzadeh, S., Schuetz, M.A., Wagels, M., and Hutmacher, D.W. Convergence of scaffold-guided bone reconstruction and surgical vascularization strategies-a quest for regenerative matching axial vascularization. Front Bioeng Biotechnol **7,** 448, 2019.
31. Vidal, L., Kampleitner, C., Brennan, M.Á., Hoornaert, A., and Layrolle, P. Reconstruction of large skeletal defects: current clinical therapeutic strategies and future directions using 3D printing. Front Bioeng Biotechnol **8,** 61, 2020.
32. Willems, W.F., Kremer, T., Friedrich, P., and Bishop, A.T. Surgical revascularization induces angiogenesis in orthotopic bone allograft. Clin Orthop Relat Res **470,** 2496, 2012.
33. Kandinata, N., and Van Fossen, K. Anatomy, Abdomen and Pelvis, Epigastric Artery. Treasure Island, FL: StatPearls Publishing, 2021.
34. Burdick, T.R., Hoffer, E.K., Kooy, T., *et al.* Which arteries are expendable? The practice and pitfalls of embolization throughout the body. Semin Intervent Radiol **25,** 191, 2008.
35. Bruyas, A., Lou, F., Stahl, A.M., *et al.* Systematic characterization of 3D-printed PCL/β-TCP scaffolds for biomedical devices and bone tissue engineering: influence of composition and porosity. J Mater Res **33,** 1948, 2018.
36. Bruyas, A., Moeinzadeh, S., Kim, S., Lowenberg, D.W., and Yang, Y.P. Effect of electron beam sterilization on three-dimensional-printed polycaprolactone/beta-tricalcium phosphate scaffolds for bone tissue engineering. Tissue Eng Part A **25,** 248, 2019.
37. Kang, J.-H., Kaneda, J., Jang, J.-G., *et al.* The influence of electron beam sterilization on in vivo degradation of β-TCP/PCL of different composite ratios for bone tissue engineering. Micromachines **11,** 273, 2020.
38. DeBaun, M.R., Stahl, A.M., Daoud, A.I., *et al.* Preclinical induced membrane model to evaluate synthetic implants for healing critical bone defects without autograft. J Orthop Res Off Publ Orthop Res Soc **37,** 60, 2019.
39. Kim, S., Bedigrew, K., Guda, T., *et al.* Novel osteoinductive photo-cross-linkable chitosan-lactide-fibrinogen hydrogels enhance bone regeneration in critical size segmental bone defects. Acta Biomater **10,** 5021, 2014.
40. Ang, L.P.K., Cheng, Z.Y., Beuerman, R.W., Teoh, S.H., Zhu, X., and Tan, D.T.H. The development of a serum-free derived bioengineered conjunctival epithelial equivalent using an ultrathin poly(epsilon-caprolactone) membrane substrate. Invest Ophthalmol Vis Sci **47,** 105, 2006.
41. Gupta, D., Singh, A.K., Kar, N., Dravid, A., and Bellare, J. Modelling and optimization of NaOH-etched 3-D printed PCL for enhanced cellular attachment and growth with minimal loss of mechanical strength. Mater Sci Eng C Mater Biol Appl **98,** 602, 2019.
42. Bhandari, M., Guyatt, G.H., Swiontkowski, M.F., Tornetta, P., 3rd, Sprague, S., and Schemitsch, E.H. A lack of consensus in the assessment of fracture healing among orthopaedic surgeons. J Orthop Trauma **16,** 562, 2002.
43. Corrales, L.A., Morshed, S., Bhandari, M., and Miclau, T. 3rd. Variability in the assessment of fracture-healing in orthopaedic trauma studies. J Bone Joint Surg Am **90,** 1862, 2008.
44. Morshed, S., Corrales, L., Genant, H., and Miclau, T. 3rd. Outcome assessment in clinical trials of fracture-healing. J Bone Joint Surg Am **90 Suppl 1,** 62, 2008.
45. Kawai, T., Shanjani, Y., Fazeli, S., *et al.* Customized, degradable, functionally graded scaffold for potential treatment of early stage osteonecrosis of the femoral head. J Orthop Res Off Publ Orthop Res Soc **36,** 1002, 2018.
46. Pearson, H.B., Mason, D.E., Kegelman, C.D., *et al.* Effects of bone morphogenetic protein-2 on neovascularization during large bone defect regeneration. Tissue Eng Part A **25,** 1623, 2019.
47. Langenfeld, E.M., and Langenfeld, J. Bone morphogenetic protein-2 stimulates angiogenesis in developing tumors. Mol Cancer Res **2,** 141, 2004.
48. Zuo, W.-H., Zeng, P., Chen, X., Lu, Y.-J., Li, A., and Wu, J.-B. Promotive effects of bone morphogenetic protein 2 on angiogenesis in hepatocarcinoma via multiple signal pathways. Sci Rep **6,** 37499, 2016.

Address correspondence to:
Yunzhi P. Yang, PhD
Department of Orthopedic Surgery
Stanford University
240 Pasteur Drive, BMI 258
Stanford, CA 94304
USA

E-mail: ypyang@stanford.edu

Received: March 8, 2021
Accepted: April 14, 2021
Online Publication Date: June 18, 2021